Applied Surface Science 585 (2022) 152756

Contents lists available at ScienceDirect

Applied Surface Science

journal homepage: www.elsevier.com/locate/apsusc

Full Length Article

Effects of Cs^+ and Ar_n^+ ion bombardment on the damage of graphite crystals

Stefania De Rosa [a,b], Paolo Branchini [a,c], Valentina Spampinato [d], Alexis Franquet [d], Gianlorenzo Bussetti [e], Luca Tortora [a,c,f,*]

[a] LASR3 Surface Analysis Laboratory INFN Roma Tre, via della Vasca Navale 84, Rome, Italy
[b] INFN, Roma Tre, via della Vasca Navale 84, Rome, Italy
[c] CNR-IMM, via del Fosso del Cavaliere 100, Rome, Italy
[d] Imec, Kapeldreef 75, B-3001, Leuven, Belgium
[e] Department of Physics, Politecnico di Milano, Piazza Leonardo da Vinci 32, I-20133 Milano, Italy
[f] Department of Science, Roma Tre University, via della Vasca Navale 84, Rome, Italy

ARTICLE INFO

Keywords:
ToF-SIMS
Graphene
Graphite
HOPG
Depth profiling

ABSTRACT

Intercalation mechanisms and diffusion or segregation phenomena in graphitic materials play a crucial role in different applied science fields. The investigation of such phenomena is usually accomplished through depth profiling experiments. Ar-GCIBs (Argon- Gas Cluster Ion Beams) are commonly adopted for in-depth concentration profiling of organic or soft materials; on the other hand, cesium ions are in general more suitable for the sputtering of inorganics. During such experiments, the beam-target interaction could alter chemistry and structure of the material. In this work, we define the optimal conditions in terms of both sputtering ion source and energy to preserve the crystal features. HOPG was used as a model system to compare morphological, physical, and chemical effects induced by different Ar_n^+ clusters, and ultra-low energy Cs^+ beam during ToF-SIMS (Time of Flight Secondary Ion Mass Spectrometry) depth profiling experiments. We demonstrated, through *in-situ* AFM (Atomic Force Microscopy) analysis, that the monoatomic Cs^+ beam alters to a lower extent the HOPG structure. On the contrary, Ar-GCIBs strongly modify the graphite surface basal plane and underlying layers. However, HOPG crystals treated with the cesium monoatomic source undergo a chemistry modification leading to the formation of graphite oxide (GOx) together with the presence of hydrogen, and cesium adducts.

1. Introduction

Graphite is an attractive material for a wide range of technological applications, mostly related to the energy storage field [1–3]. The original properties of graphitic materials can be changed by means of a great variety of physical and chemical processes, according to specific applicative purpose. Just to mention a well-known example, the chemical manipulation of HOPG crystals for defect-free graphene production through exfoliation involved significant efforts [4,5], being HOPG the conventional ordered crystal composed of stacked graphene layers [6]. In this context, being able to reveal any sort of modification induced on pristine graphite is a mandatory task. Complementary surface analysis techniques like X-ray Photoelectron Spectroscopy (XPS) [4], Scanning Tunneling Microscopy (STM) [7], AFM (Atomic Force Microscopy) [8,9], and Raman spectroscopy [10], were adopted to study surface morphology and structure of graphitic samples. XPS and ToF-SIMS (Time of Flight Secondary Ion Mass Spectrometry) experiments even more often involve the use of ion beams to explore in depth graphite-based systems [4,11–19]. ToF-SIMS depth profiling experiments were already employed to investigate diffusion phenomena, contamination, and damage effects on hybrid organic/inorganic electronic devices [20,21], polymers [22], and semiconductors [23]. In a recent work, we used ToF-SIMS dual-beam depth profiling analysis, combined with *in-situ* AFM measurements, to identify oxidative products and structural defects inside HOPG crystals treated with standard electrochemical routines in mild acid solutions [11]. In this kind of experiments, the effects of the interaction between accelerated ions and target must be considered; experimental parameters such as energy, current density,

* Corresponding author at: LASR3 (Surface Analysis Laboratory Roma tre) INFN & Roma Tre University, via della Vasca Navale 84, Rome, Italy. Tel.: +390657337261.
E-mail address: luca.tortora@uniroma3.it (L. Tortora).

https://doi.org/10.1016/j.apsusc.2022.152756
Received 21 October 2021; Received in revised form 25 January 2022; Accepted 4 February 2022
Available online 7 February 2022

fluence must be tuned according to the specific case study. In addition, for what regards the sputtering ion beam it is also required the optimization of ion yield, depth resolution, and sputter rate. The choice of the ion specie to adopt, fitting to a large spectrum of targets, ranging from inorganic to organic samples is a long-standing issue in the SIMS community. Graphite is a carbon-based compound but it is commonly classified as inorganic, therefore the selection of the ion source for depth profiling analysis of such materials can be not trivial. Large cluster ion beams (e.g., Ar_n^+ clusters with n = 250–10000) quickly became very widespread as sputter sources for organic/polymer surfaces and devices [24,25]. It was demonstrated, by detailed simulation studies, that the impact of massive clusters on the target induces minimal molecular degradation and fragmentation compared to smaller projectiles[26]. However, the use of Ar-GCIB as analysis beam could be limited by low mass resolution and accuracy and, sometimes, low ionization efficiency [26]. On the other hand, the Cs^+ beam is characterized by its capacity to sputter away organic and inorganic materials with similar erosion rates, high negative ionization yield for molecular species, and the property of reducing chemical modifications during the sputtering process[27]. Several comparative studies, performed by varying parameters such as beam energy, ion fluence, or target temperature were already carried out on hybrid organic/inorganic layered systems[28] or graphitic materials [14,29]. At the same way, in the present work, we aim to rationalize the ion beam-induced undesired effects on HOPG crystals when ToF-SIMS depth profiles experiments are performed with Ar-GCIBs or Cs^+ as sputtering beams. Standard pristine HOPG was sputtered with low-energy Cs^+ ions and with Ar_n^+ cluster ions, the latter with two different energy-per-atom (E/n) values, then gun-induced surface alterations were observed with *in-situ* AFM measurements. The morphological changes due to the ion impact on the sample surface and the chemical alteration related to the ion-target interaction strongly depend on the sputtering ions species and energy.

2. Experimental section

2.1. Materials

The z-grade pristine HOPG samples (10 mm × 10 mm × 2 mm) were purchased from Optigraph. The surface of HOPG was prepared by peeling several times using adhesive tape before each measurement.

2.2. In-situ ToF-SIMS/AFM analysis

HOPG crystals were analyzed with a ToF-SIMS/AFM integrated tool (ToF-SIMS NCS, IONTOF GmbH, Münster, Germany), in which ToF-SIMS and AFM instrumentations are combined in the same UHV analysis chamber. In such a system the sample stage can be moved between the ToF-SIMS and AFM unit through a high-speed piezo-driven stage with sub-μm position accuracy. The transfer of the sample stage to the AFM position after suspension of the ToF-SIMS depth profile experiment is made without breaking the vacuum. In this way, it is possible to analyze the same region of the sample with both techniques and with different types of sputtering beams. During the sample stage transfer, the sub-μm positioning precision and accuracy are guaranteed by the stage calibration. ToF-SIMS dual-beam depth profiling was performed on HOPG sample using a bunched Bi_1^+ gun at high-energy (30 keV) and low-current (~1 pA) as primary beam. Low-energy and high-current $Ar_n^+$and Cs^+ beams were used as sputtering guns. The experimental parameters adopted for the sputtering guns, summarized in Table 1, were chosen in order to compare different sputtering conditions at different ion energies. The two E/n values of the Ar_n^+ beams have been reached starting from clusters of similar size and doubling the total energy. Relatively small cluster sizes for Ar_n^+ beams were chosen in order to allow a relatively fast sputtering process. The current values were optimized in order to improve the erosion rate of the Ar_n^+ gun, and the ionization yield of the Cs^+ beam. Dual-beam depth profiling analysis was conducted in interlaced mode[30]. In the interlaced mode, the sample is bombarded with a bismuth liquid metal ion gun that provides short pulses (<1ns) of single or cluster (Bi_3^{++}, Bi_5^{++}) ions able to desorb and ionize elements and molecules at the sample surface; at the same time, between analysis pulses, the sputtering beam (Cs^+ or Ar_n^+) is active removing sample surface material layer by layer and operating quasi-simultaneously and quasi-continuously on the target analysis area. The ion bombardment experiments were performed at room temperature, as revealed by the temperature sensor installed in the analysis chamber (25–30 °C). The experimental setup does not allow to directly monitor possible local temperature increase of the target irradiated area. The Bi_1^+ gun analysis area of 100 μm × 100 μm was set at the center of the sputtering area of 300 μm × 300 μm. As the analysis is destructive, each ToF-SIMS depth profile was acquired in different areas of the sample surface. *In-situ* AFM measurements in contact mode were obtained on the analyzed area after each depth-profiling measurement. In these studies, IMEC heavily boron-doped diamond probes mounted on a cantilever with a nominal spring constant of 27 N/m were used. Images were scanned with a scan speed of 5 μm/s.

Table 1
Experimental parameters of sputter beams in ToF-SIMS depth profile experiments: cluster size, energy, energy-per-atom, and ion currents.

Sputtering ion species	E (keV)	E/n (eV)	Ion current (nA)
Ar^+_{1000}	20	~ 20	~ 10
Ar^+_{1300}	10	~ 8	~ 4
Cs^+	0.250	250	~ 15

3. Results and discussion

The AFM surface images of 16 μm × 16 μm were acquired at the center of the HOPG analysis area in order to evaluate the morphological changes introduced by the ion bombardment experiments performed in dual-beam mode with Cs^+ at 250 eV, Ar_n^+ cluster at 10 keV (E/n ~ 8 eV), and Ar_n^+ cluster at 20 keV (E/n ~ 20 eV) as sputter beams. The fluence value reached during the measurements (~4×10^{17} ions/cm^2) is the same for the three cases, in order to avoid possible differences in the target morphology induced by the fluence variation. The ion current and/or the ion beam fluence, i.e. the number of ions arriving to the target surface per unit time, is a relevant parameter in the sputtering process. At high current density values (~10^{-1} mA/cm^2), the ion beam can produce an accumulation of damages and a significant rise of the target temperature, resulting in increasing the defects recombination rate in the target material. When the temperature is kept to high values (from 90 °C to 700 °C), it was demonstrated that ion-induced structural, emission, and morphological changes are influenced by temperature variations of graphitic samples [29,31]. In these cases, the self-annealing process, competing with the ion irradiation damage, should be considered. However, all ion beam bombardment experiments were conducted at room temperature in this study. In Fig. 1, the HOPG surface sputtered with the three conditions (Fig. 1b-d) can be compared to the pristine HOPG surface (Fig. 1a). Here, the typical HOPG surface features (e.g., terraces and steps) are visible, and the surface roughness is in the sub-nanometer range. When graphite interacts with the ultra-low energy Cs^+ impinging ions (Fig. 1b), drifts and micro/nano-metric hillocks, probably present below the surface, are brought to light. The bare HOPG basal plane still presents the regularity of the pristine surface, despite an appreciable increase in the roughness visible in the scan profile. Otherwise, after the Ar cluster bombardment, the HOPG surface morphology dramatically changes. In Fig. 1c, it emerges that Ar^+_{1300} ions with an impacting energy-per-atom of ~ 8 eV, drastically alter the HOPG surface morphology. At the end of the depth profiling measurement, the surface roughness is at least one order of magnitude highest with respect to the not bombarded sample. A dense pattern of widespread micrometric reliefs characterizes the AFM image in Fig. 1c. For

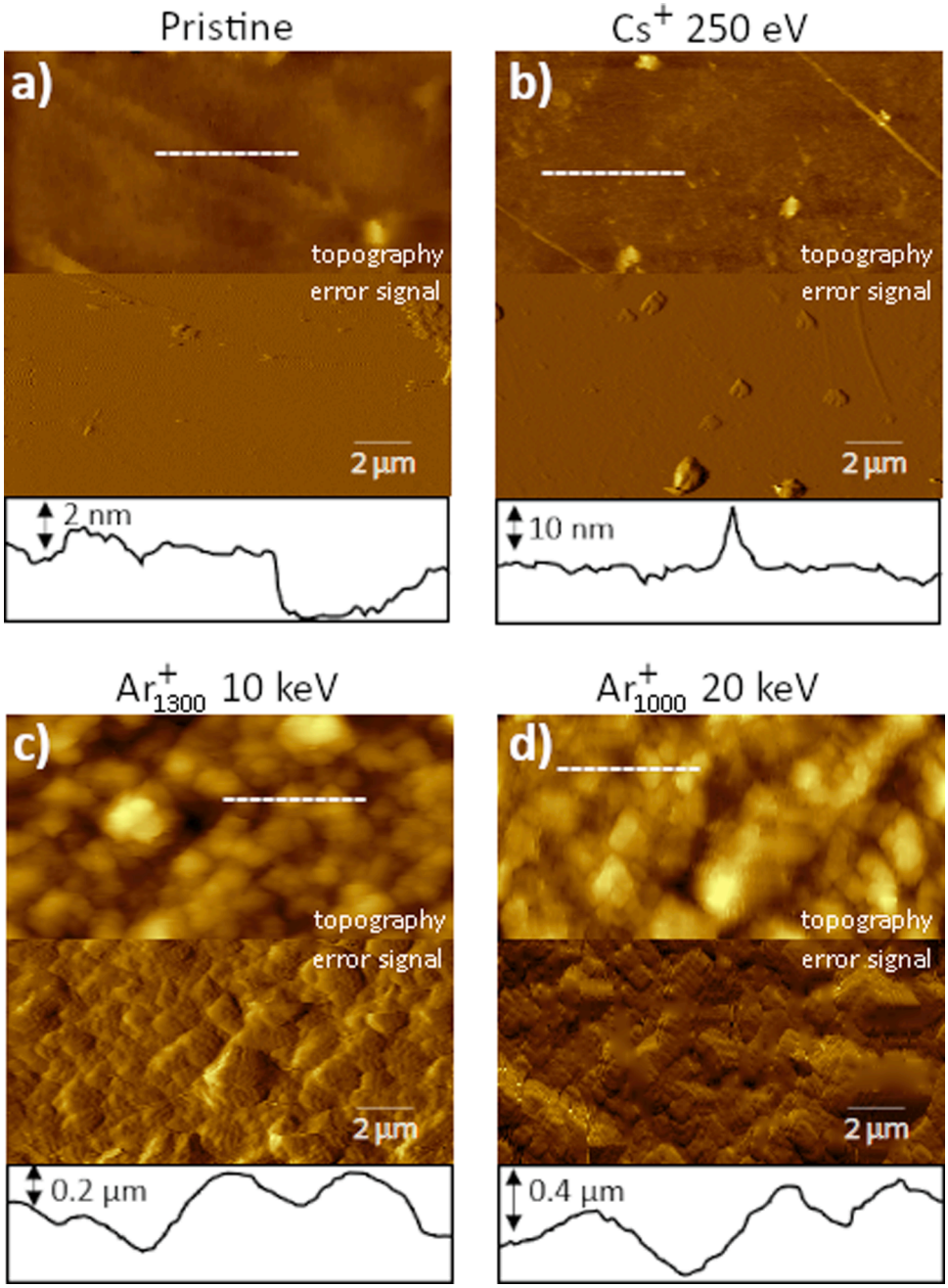

Fig. 1. AFM images (16 µm × 16 µm) acquired on (a) pristine HOPG surface, and HOPG surface after ion-induced sputtering with (b) Cs^+ beam at 250 eV (c) Ar^+_{1300} cluster beam at 10 keV, and (d) Ar^+_{1000} cluster beam at 20 keV with a fluence of ~ 4×10^{17} ions/cm^2. The surface profiles are acquired along the white dashed lines depicted inside each image. Topography (up) vs error signal (down) are shown in all images .

the Ar_{1000}^+ gun at E/n ~ 20 eV, the outcome is almost the same. The surface roughness after the sputtering is very high (tens of nanometers), and the HOPG surface is heavily damaged (Fig. 1d). Both Ar-GCIBs used as sputtering sources seem to strongly alter the pristine HOPG morphology. It was found, in molecular dynamics simulation works[32], that the collisional process of cluster ions depends on the local surface morphology of the target. The surface roughness changes according to the shape of the impact point, especially when the analyzed area has similar scale with the pristine structure of the sample. Many experimental studies demonstrated that the parametric threshold to cause surface damage with gas cluster ion beams is mainly dominated by the E/n value[33,34]. The energy-per atom values of the Ar^+ guns used in the present work are relatively close to the carbon bond dissociation energy in graphite (~10.3 eV). A sputtering ion gun with low energy-per-atom should not cause dramatic structural damages, but its interaction with the bombarded surface can alter its morphology through decomposition or desorption effects[32]. The sputtering yield is also correlated to this energy threshold. In this work, the three sputtering species hit the target with the same incident angle (45° with respect to the sample plane) so, looking at the comparison among the surface morphology in Fig. 1, it is possible to assume that the interaction of energetic charged particles with ordered graphite crystal can modify its morphological features more or less dramatically, depending on the impinging single-particle energy. The HOPG sample appears most affected by the Ar^+ ion clusters, with small energy-per-ion values compared to the monoatomic Cs^+ gun at 250 eV, in terms of morphological damage. The experimental sputtering yield values obtained in this work are affected by a significant error and it is not attainable to

precisely compare them with values present in the literature. In Seah's work[35] the yield of atoms sputtered by Ar-GCIBs is described with a simple universal equation, supported by experimental results for elementary materials and organic/inorganic compounds, but not for graphite samples. For depth-profiling analysis of layered crystals such as HOPG, the adopted sputtering ion beam must gently remove the crystal sheets, especially if the aim is to detect intercalated species within the interlayer space. The penetration of the sputtering ions in the sub-surface regions of the target can modify the chemical configuration of the hosting materials. It is essential to understand the extent of such chemical alteration in order to further refine the adopted experimental conditions.

ToF-SIMS secondary ion mass spectra (m/z = 0–250) obtained with the three sputtering ion species in negative polarity are shown in Fig. 2. The plotted spectra correspond to the averaged result collected during the depth profiling measurements over four different analysis areas. The intensity counts were integrated up to the same fluence value (~4 × 10^{17} ions/cm^2). As expected, the mass spectra of HOPG crystal, just cleaved by adhesive tape and then analyzed in the ultra-high vacuum chamber, are basically dominated by the C_n^- (n = 1, 2..) fragment ions, when the sputtering is made with Ar^+ cluster beams, as shown in Fig. 2a, b. Here, only a slight difference in intensity can be noticed, according to the two distinct E/n values. The mass spectrum resulting from the Cs^+ gun sputtering, in Fig. 2c, exhibits the C_n^- series, a pretty intense H^- ion peak, and, at high mass values, multiple cesium-carbon adducts. In addition, the O^- ion peak appears more pronounced. As argued in previous works[4,12], ionized C_n^- fragments with small n come from the direct breaking up of defect-free areas of HOPG crystal, but also from secondary crumbling of ions with higher n values which, for this reason, have generally lower intensities in the mass spectra. Possible differences between the C_n^- (n = 3 – 12) ion fragments from Cs^+- and Ar^+-bombarded HOPG can be evaluated normalizing their intensities with respect to the total counts. The intensity trend of the C_n^- ion series, in Fig. 3, exponentially decreases with the number n of the carbon atoms. In addition, an oscillating modulation of the intensity between even and odd n values appears, having the even carbon clusters higher normalized intensities with respect to the adjacent C_n^- fragments with an odd n. These findings are in agreement with some theoretical predictions about the C_n^- clusters ($n \leq 10$) stability, based on the functional density (DFT) method, and also supported by experimental results [36]. Deviation from the predicted oscillatory trend is attributed to a chain-to-ring transformation of the carbon clusters[36]. In Fig. 3 such a deviation is visible starting from $n \geq 9$. The general trend of the C_n^- ion series appears to be similar for the three sputtering species. However, the C_n^- secondary ions with greater molecular weight ($n \geq 7$) have higher intensities when the sputtering gun is Ar_{1000}^+ at 20 keV. This result is in agreement with the assumption that ion cluster beams generate with low probability small fragments, leaving molecules with high molecular weight intact during the sputtering[37]. The H^- secondary ions in the mass spectrum of HOPG sputtered with Cs^+ at 250 eV could denote the presence of defects. The formation probability of hydrogen-containing secondary ions is higher in ultra-thin graphite layers during SIMS measurements, since low-dimensional graphitic surfaces (e.g. graphene) have generally many more defects than the surface of a bulk sample[12]. Considering the just mentioned assumption, the fact that H^- secondary ion is more intense when Cs^+ is used as sputtering beam has two possible explanations: distinguishing features from consecutive stacked graphite layers can be detected with the Cs^+ gun at ultra-low energy, or the tendency of monoatomic species to implant in the near-surface region of the bombarded target causes a partial alteration of the uppermost layers of the crystal, resulting in an enhancement of the H^- signal. The first explanation suggests that the use of ultra-low energy Cs^+ sputtering beam could provide nanometric depth resolution. Higher values of depth resolution for ultra-low energy Cs^+ sputtering beam, with respect to Ar^+ cluster beam, were already found in previous work on hybrid organic/inorganic model systems[38]. Oxygen (O^-) ions are also present

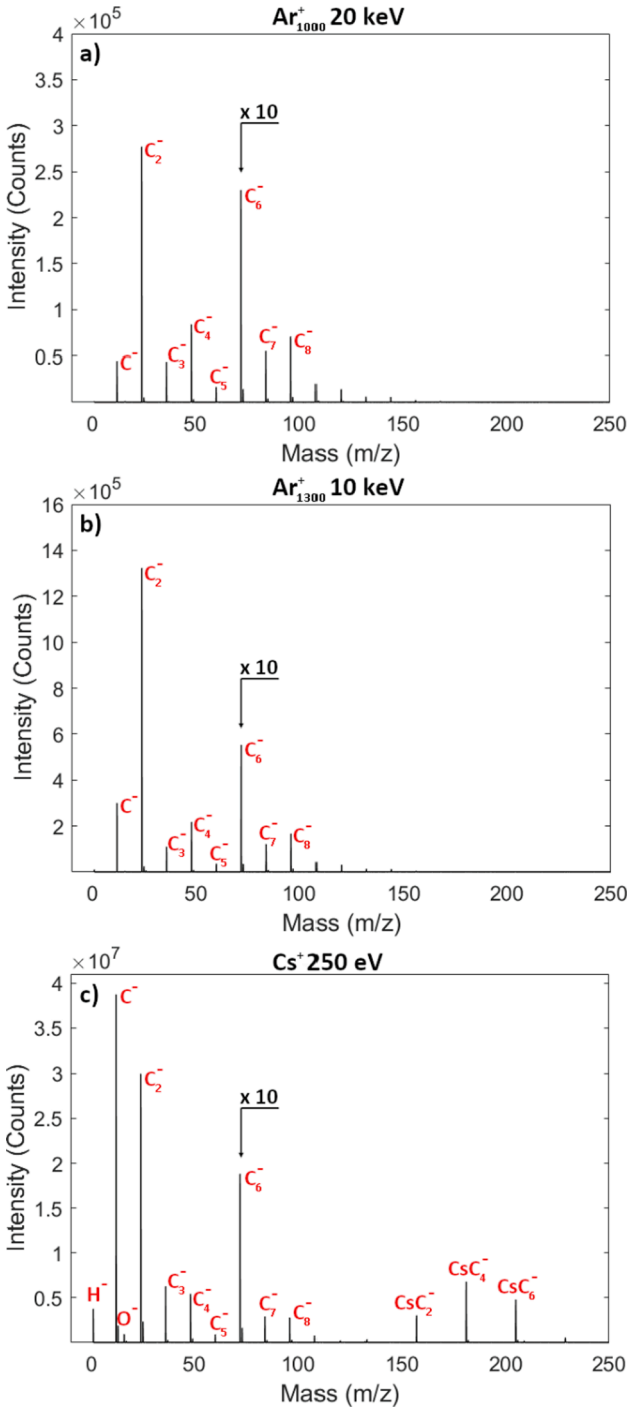

Fig. 2. Integrated ToF-SIMS negative secondary ion spectra of HOPG from depth profiling experiments with (a) Ar^+_{1000} sputter beam at 20 keV, (b) Ar^+_{1300} sputter beam at 10 keV, and (c) Cs^+ sputter beam at 250 eV.

in the HOPG mass spectra in Fig. 2. GOx formation could mean a chemical change of the sample triggered by its interaction with energetic ions that are implanted[7,14]. Such undesired effect seems to be more pronounced when Cs^+ gun is used, since the intensity of the O^- ion signal is considerably higher in the mass spectrum of Cs-bombarded HOPG. However, it is not possible to discern with certainty whether the increase of the oxygen content in the HOPG mass spectrum is an ion species-dependent effect, or if it is only due to the higher negative ion sputter yield of the Cs^+ beam for the O^- ions already present the crystal. The CsC_n^- peaks in Fig. 2c can be due to a process similar to the MCs^+

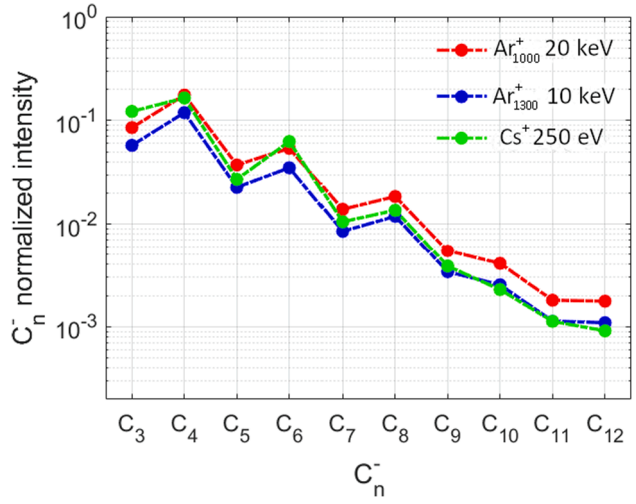

Fig. 3. Logarithmic-scale plot of the normalized intensity of Cn– (n = 3–12) ion series from ToF-SIMS mass spectra. Red, blue, and green curves refer to Ar1000 + cluster at 20 keV, Ar1300 + cluster at 10 keV, and Cs + at 250 eV sputter beams, respectively.

secondary ions formation, when an independently sputtered neutral atom recombines to a re-sputtered Cs^+ atom in the proximity of the sample surface. The MCs^+ species slightly suffer from the so-called matrix effect and are used to measure the atomic concentration of the element M in the analyzed sample[39]. As already mentioned, the Cs^+ ions can implant into HOPG as interstitial defects between the graphite basal planes, having cesium ion a diameter of 3.38 Å, comparable with the HOPG layer spacing (3.35 Å). ToF-SIMS depth profiles obtained with Ar_n^+ cluster beam at E/n ~ 20 eV, ~ 8 eV, and Cs^+ beam at 250 eV are shown in Fig. 4. C_6^- ($m/z = 72$), O^- ($m/z = 16$), and H^- ($m/z = 1$) ion signal intensities from HOPG are plotted versus the same fluence value (~4 × 10^{17} ions/cm^2). Cs^- ion signal is also shown in Fig. 4c. The intensity signals are averaged over four measurements acquired in different analysis areas. The C_6^- ion signal is commonly used as a reference for graphite-based samples[12,40,41], while the O^- and H^- ions were chosen as markers of matrix oxidation and structural defects inside the crystal. The secondary ion intensity profiles obtained with the ultra-low energy Cs^+ gun are at least one order of magnitude higher than the same ion profiles obtained with the Ar^+ clusters. Such effect may be related to the enhancement of the ionization yield of the negatively charged sputtered ions typical of the Cs^+ source[42]. For what concerns the O^- and H^- signals, surface defects were detected with the three sputtering beams, as the starting values of the blue and green profiles in Fig. 4 confirm. O^-/C_6^- intensity ratios from depth profiles obtained with Cs^+ at 250 eV (green curve), Ar^+_{1300} at 10 keV (blue curve), and Ar^+_{1000} at 20 keV (red curve) are plotted versus the ion fluence (~4 × 10^{17} ions/cm^2) in Fig. 5.

In the three cases the sputtering result in an initial rapid decrease of the surface oxygen. Interestingly, the O^- signal remains intense as the surface is sputtered away, suggesting that it is also present in the near-surface areas of the crystal. This is more evident in the O^-/C_6^- ratio from depth profiles obtained with Cs^+ at 250 eV and Ar^+_{1300} at E/n ~ 8. O^-/C_6^- ratio from the HOPG sample sputtered with Ar^+_{1000} at 20 keV goes to negligible values before the end of the measurement. Once the steady state of the signals is reached, at fluence value of about 10^{17} ions/cm^2, the depth profiles obtained with the Cs^+ gun are more stable and intense, up to the sample sub-surface regions. The 3D reconstruction of O^- secondary ions spatial distribution within the HOPG bulk, sputtered with the three guns, are shown in Fig. 6. The three data cubes, obtained by stacking along the sputtering direction consecutive analysis images (100 μm × 100 μm), show circular high-intensity spots within the crystal planes bombarded at the lower fluence values, at the start of the

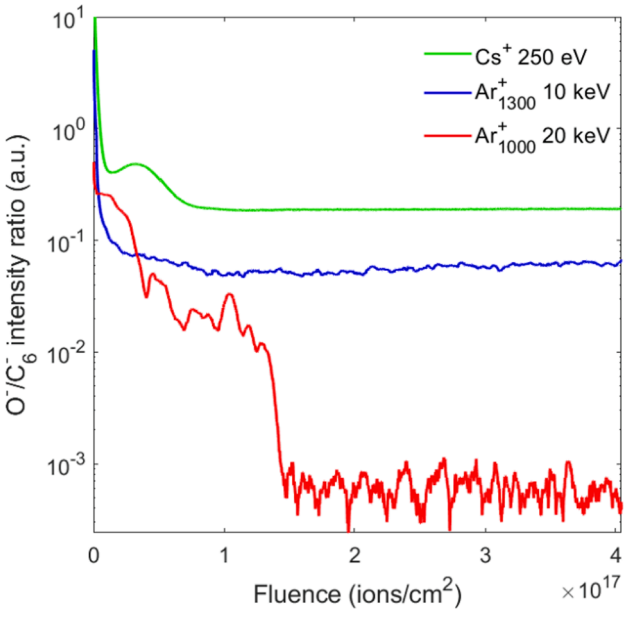

Fig. 5. Intensity ratios between O^- and C_6^- ion signals of depth profiling obtained with Ar^+_{1000} at 20 keV (red curve), Ar^+_{1300} at 10 keV (blue curve), and Cs^+ at 250 eV (green curve) as sputtering guns for the HOPG sample.

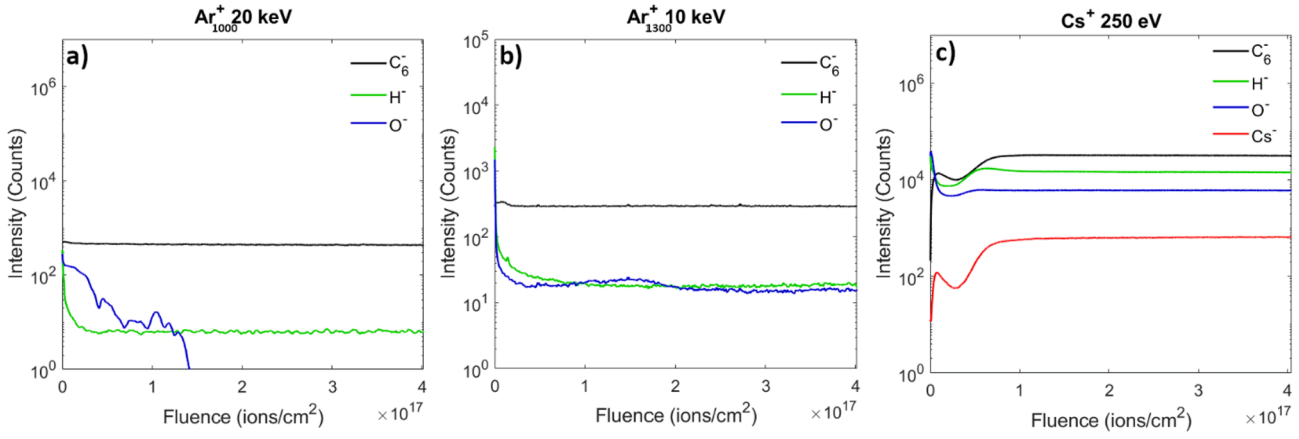

Fig. 4. ToF-SIMS depth profiles of HOPG obtained with (a) Ar^+_{1000} at 20 keV, (b) Ar^+_{1300} at 10 keV, and (c) Cs^+ at 250 eV as sputtering beams. Secondary ion intensities of C_6^- ($m/z = 72$), H^- ($m/z = 1$), and O^- ($m/z = 16$) are plotted versus the fluence. Cs^- ($m/z = 132.9$) ion intensity is also shown in (c).

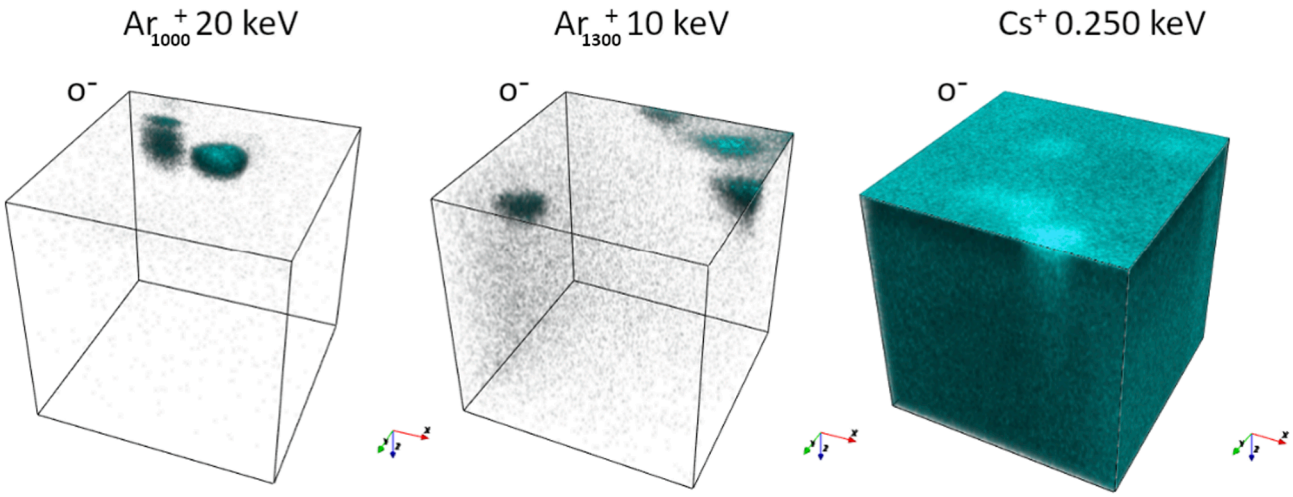

Fig. 6. 3D ion distributions reconstructed from ToF-SIMS dual beam depth profiling measurements on HOPG. O− (m/z = 16) ion distributions is shown for Ar + 1000 cluster at 20 keV (left), Ar + 1300 cluster at 10 keV (central), and Cs + at 250 eV (right).

measurements. Oxygen-based secondary ions, extending far below the surface and following crystal crack and rifts within the basal planes, have been observed with depth profiling experiments using low-energy Cs^+ sputtering beam[11]. The O^- background signal in the HOPG matrix sputtered with the Cs^+ gun is hugely more intense up to the end of the depth profiling measurement, while the signal goes to zero when Ar^+ cluster guns are used. With the monoatomic sputtering source it is still possible to appreciate spots of greater intensity due to possible structural defects and cracks. The uniformly distributed O^- background signal is a consequence of the enhancement of the ionization yield for negatively charged sputtered secondary ions, typical of the Cs^+ bombarding beam [42].

4. Conclusions

Pristine HOPG was depth profiled through dual-beam ToF-SIMS experiments with ultra-low energy Cs^+ beam and Ar^+ cluster beams, with different cluster sizes and energies, as sputtering guns. Unexpectedly, the modification of the topological features seems to be related to the impinging particle energy more than the projectile size. Argon cluster sources at 10 and 20 keV, with energy-per-atom values ranging from 8 to 20 E/n values, were found to be more destructive for the HOPG surface structure than ultra-low energy (250 eV) cesium. The beam-induced matrix oxidation and the implantation of atoms originating from the ionic probe must be taken into account when the Cs^+ gun is used. However, due to the excellent intensity yield of the negative ion signals found when using ultra-low energy Cs^+, the latter would be the optimal choice for layered systems like HOPG. On the other hand, the Ar^+ cluster sources leave heavier carbon-based rings intact during the sputtering and this should make it suitable for low-dimensional systems, like few-layer graphene stacks. All these findings can be helpful in guiding the choice of the sputtering beam conditions in a wider range of graphite-based materials and devices.

CRediT authorship contribution statement

Stefania De Rosa: Investigation, Formal analysis, Data curation, Software, Methodology, Writing – original draft. **Paolo Branchini:** Resources, Funding acquisition, Writing – review & editing. **Valentina Spampinato:** Investigation, Formal analysis, Methodology, Writing – review & editing. **Alexis Franquet:** Funding acquisition, Investigation, Formal analysis, Methodology, Writing – review & editing. **Gianlorenzo Bussetti:** Validation, Writing – review & editing. **Luca Tortora:** Project administration, Funding acquisition, Conceptualization, Supervision, Writing – review & editing.

Declaration of Competing Interest

The authors declare that they have no known competing financial interests or personal relationships that could have appeared to influence the work reported in this paper.

Acknowledgments

The TOF-SIMS/AFM instrument was financially supported by the HERCULES foundation (now FWO). Part of this project has received funding from the European Union's Horizon 2020 research and innovation program under Grant Agreement No.688225 (Metro4-3D). This work has been partially funded by the Italian Ministry of University and Research in the framework of the Premial Project EOS (Organics Electronics for Innovative Research Instrumentation). LASR3 Surface Analysis Laboratory Roma Tre gratefully acknowledges financial support from "Fondazione Roma" (Grant 5229441F37). The sample preparation has been performed in the Solid − Liquid Interface and Nanomicroscopy (SoLINano) lab that is an inter-Departmental facility of the Politecnico di Milano.

References

[1] B.A. Ali, A.H. Biby, N.K. Allam, Toward the Proper Selection of Carbon Electrode Materials for Energy Storage Applications: Experimental and Theoretical Insights, Energy & Fuels. 35 (16) (2021) 13426–13437, https://doi.org/10.1021/acs.energyfuels.1c01528.
[2] X. Li, J. Li, L. Ma, C. Yu, Z. Ji, L. Pan, W. Mai, Graphite Anode for Potassium Ion batteries: Current Status and Perspective, ENERGY \& Environ. Mater. n/a (n.d.). https://doi.org/https://doi.org/10.1002/eem2.12194.
[3] H. Zhang, Y. Yang, D. Ren, L. Wang, X. He, Graphite as anode materials: Fundamental mechanism, recent progress and advances, Energy Storage Mater. 36 (2021) 147–170, https://doi.org/10.1016/j.ensm.2020.12.027.
[4] W. Xie, L.-T. Weng, K.L. Yeung, C.-M. Chan, Repair of defects created by Ar+ sputtering on graphite surface by annealing as confirmed using ToF-SIMS and XPS, Surf. Interface Anal. 50 (9) (2018) 851–859, https://doi.org/10.1002/sia.6487.
[5] M.J. Webb, P. Palmgren, P. Pal, O. Karis, H. Grennberg, A simple method to produce almost perfect graphene on highly oriented pyrolytic graphite, Carbon N. Y. 49 (10) (2011) 3242–3249, https://doi.org/10.1016/j.carbon.2011.03.050.
[6] K.S. Novoselov, D. Jiang, F. Schedin, T.J. Booth, V.V. Khotkevich, S.V. Morozov, A. K. Geim, Two-dimensional atomic crystals, Proc. Natl. Acad. Sci. 102 (30) (2005) 10451–10453, https://doi.org/10.1073/pnas.0502848102.
[7] Y. Zhu, J.D. McBride, T.A. Hansen, T.P. Beebe, Controlled production of molecule corrals using cesium ion bombardment: A TOF-SIMS, XPS, and STM Study, J. Phys. Chem. B. 105 (2001) 2010–2018, https://doi.org/10.1021/jp0040300.
[8] D. Alliata, R. Kötz, O. Haas, H. Siegenthaler, In Situ AFM Study of Interlayer Spacing during Anion Intercalation into HOPG in Aqueous Electrolyte, Langmuir. 15 (24) (1999) 8483–8489, https://doi.org/10.1021/la990402o.

[9] G. Bussetti, L. Duò, Anion Intercalation in Graphite Studied by Electrochemical-Scanning Probe Microscopy: State of the Art and Perspectives, in: K. Wandelt (Ed.), Encycl, Interfacial Chem, Elsevier, Oxford, 2018, pp. 27–37, https://doi.org/10.1016/B978-0-12-409547-2.14164-2.
[10] N. Kumar, S. Marchesini, T. Howe, L. Edwards, B. Brennan, A.J. Pollard, Nanoscale characterization of plasma functionalized graphitic flakes using tip-enhanced Raman spectroscopy, J. Chem. Phys. 153 (18) (2020) 184708, https://doi.org/10.1063/5.0024370.
[11] S. De Rosa, P. Branchini, V. Spampinato, A. Franquet, R. Yivlialin, L. Duò, G. Bussetti, L. Tortora, Stratigraphic analysis of intercalated graphite electrodes in aqueous inorganic acid solutions, Nano Res. 15 (2) (2022) 1120–1127, https://doi.org/10.1007/s12274-021-3614-6.
[12] W. Xie, L.-T. Weng, K.M. Ng, C.K. Chan, C.-M. Chan, Defects of clean graphene and sputtered graphite surfaces characterized by time-of-flight secondary ion mass spectrometry and X-ray photoelectron spectroscopy, Carbon N. Y. 112 (2017) 192–200, https://doi.org/10.1016/j.carbon.2016.11.002.
[13] S. De Rosa, P. Branchini, R. Yivlialin, L. Duò, G. Bussetti, L. Tortora, Disclosing the Graphite Surface Chemistry in Acid Solutions for Anion Intercalation, ACS Appl. Nano Mater. 3 (1) (2020) 691–698, https://doi.org/10.1021/acsanm.9b0222010.1021/acsanm.9b02220.s001.
[14] A. Theodosiou, B.F. Spencer, J. Counsell, A.N. Jones, An XPS/UPS study of the surface/near-surface bonding in nuclear grade graphites: A comparison of monatomic and cluster depth-profiling techniques, Appl. Surf. Sci. 508 (2020), 144764, https://doi.org/10.1016/j.apsusc.2019.144764.
[15] Z. Wang, H. Yang, Y. Liu, Y. Bai, G. Chen, Y. Li, X. Wang, H. Xu, C. Wu, J. Lu, Analysis of the Stable Interphase Responsible for the Excellent Electrochemical Performance of Graphite Electrodes in Sodium-Ion Batteries, Small. 16 (2020) 2003268, https://doi.org/10.1002/smll.202003268.
[16] M. Ma, A.N. Mansour, J.K. Ko, G.H. Waller, C.E. Hendricks, Characterization of Li Diffusion and Solid Electrolyte Interface for Li4Ti5O12 Electrode Cycled with an Organosilicon Additive Electrolyte, J. Electrochem. Soc. 167 (11) (2020) 110549, https://doi.org/10.1149/1945-7111/aba5d3.
[17] N. Ehteshami, L. Ibing, L. Stolz, M. Winter, E. Paillard, Ethylene carbonate-free electrolytes for Li-ion battery: Study of the solid electrolyte interphases formed on graphite anodes, J. Power Sources. 451 (2020), 227804, https://doi.org/10.1016/j.jpowsour.2020.227804.
[18] H. Jin, S. Xin, C. Chuang, W. Li, H. Wang, J. Zhu, H. Xie, T. Zhang, Y. Wan, Z. Qi, W. Yan, Y.-R. Lu, T.-S. Chan, X. Wu, J.B. Goodenough, H. Ji, X. Duan, Black phosphorus composites with engineered interfaces for high-rate high-capacity lithium storage, Science 370 (6513) (2020) 192–197.
[19] B. Rais, E.T. Ostrowski, A. Canton, C.H. Skinner, S. Barison, S. Fiameni, B.E. Koel, SIMS and HR-XPS characterization of lithiated graphite from the magnetic fusion device RFX-mod, Appl. Surf. Sci. 567 (2021), 150830, https://doi.org/10.1016/j.apsusc.2021.150830.
[20] L. Tortora, M. Urbini, A. Fabbri, P. Branchini, L. Mariucci, M. Rapisarda, M. Barra, F. Chiarella, A. Cassinese, F. Di Capua, A. Aloisio, Three-dimensional characterization of OTFT on modified hydrophobic flexible polymeric substrate by low energy Cs+ ion sputtering, Appl. Surf. Sci. 448 (2018) 628–635, https://doi.org/10.1016/j.apsusc.2018.04.097.
[21] C. Noël, L. Houssiau, Hybrid Organic/Inorganic Materials Depth Profiling Using Low Energy Cesium Ions, J. Am. Soc. Mass Spectrom. 27 (5) (2016) 908–916, https://doi.org/10.1007/s13361-016-1353-9.
[22] L. Houssiau, B. Douhard, N. Mine, Molecular depth profiling of polymers with very low energy ions, Appl. Surf. Sci. 255 (2008) 970–972, https://doi.org/10.1016/j.apsusc.2008.05.027.
[23] J.C. Lee, J. Won, Y. Chung, H. Lee, E. Lee, D. Kang, C. Kim, J. Choi, J. Kim, Investigations of semiconductor devices using SIMS; diffusion, contamination, process control, Appl. Surf. Sci. 255 (2008) 1395–1399, https://doi.org/10.1016/j.apsusc.2008.06.129.
[24] D. Rading, R. Moellers, H.-G. Cramer, E. Niehuis, Dual beam depth profiling of polymer materials: comparison of C60 and Ar cluster ion beams for sputtering, Surf. Interface Anal. 45 (2013) 171–174, https://doi.org/10.1002/sia.5122.
[25] T. Mouhib, C. Poleunis, N. Wehbe, J.J. Michels, Y. Galagan, L. Houssiau, P. Bertrand, A. Delcorte, Molecular depth profiling of organic photovoltaic heterojunction layers by ToF-SIMS: comparative evaluation of three sputtering beams, Analyst. 138 (2013) 6801–6810, https://doi.org/10.1039/C3AN01035J.
[26] N. Winograd, Gas Cluster Ion Beams for Secondary Ion Mass Spectrometry, Annu. Rev. Anal. Chem. 11 (1) (2018) 29–48, https://doi.org/10.1146/annurev-anchem-061516-045249.
[27] L. Houssiau, N. Mine, Molecular depth profiling with reactive ions, or why chemistry matters in sputtering, Surf. Interface Anal. 43 (2011) 146–150, https://doi.org/10.1002/sia.3528.
[28] C. Noël, S. Pescetelli, A. Agresti, A. Franquet, V. Spampinato, A. Felten, A. di Carlo, L. Houssiau, Y. Busby, Hybrid Perovskites Depth Profiling with Variable-Size Argon Clusters and Monatomic Ions Beams, Materials (Basel). 12 (5) (2019) 726, https://doi.org/10.3390/ma12050726.
[29] N.N. Andrianova, A.M. Borisov, E.S. Mashkova, A.A. Shemukhin, V.I. Shulga, Y. S. Virgiliev, Relief evolution of HOPG under high-fluence 30keV argon ion irradiation, Nucl. Instruments Methods Phys. Res. Sect. B Beam Interact. with Mater. Atoms. 354 (2015) 146–150, https://doi.org/10.1016/j.nimb.2014.11.071.
[30] J.C. Vickerman, D. Briggs, ToF-SIMS: surface analysis by mass spectrometry, IM, 2001.
[31] D. Liu, D. Cherns, S. Johns, Y. Zhou, J. Liu, W.-Y. Chen, I. Griffiths, C. Karthik, M. Li, M. Kuball, J. Kane, W. Windes, A macro-scale ruck and tuck mechanism for deformation in ion-irradiated polycrystalline graphite, Carbon N. Y. 173 (2021) 215–231, https://doi.org/10.1016/j.carbon.2020.10.086.
[32] T. Aoki, Molecular dynamics simulations of cluster impacts on solid targets: implantation, surface modification, and sputtering, J. Comput. Electron. 13 (1) (2014) 108–121, https://doi.org/10.1007/s10825-013-0504-5.
[33] S. Houzumi, K. Mochiji, N. Toyoda, I. Yamada, Scanning tunneling microscopy observation of graphite surfaces irradiated with size-selected Ar cluster ion beams, Japanese J. Appl. Physics, Part 1 Regul. Pap. Short Notes Rev. Pap. 44 (8) (2005) 6252–6254, https://doi.org/10.1143/JJAP.44.6252.
[34] K. Nakamura, S. Houzumi, N. Toyoda, K. Mochiji, T. Mitamura, I. Yamada, Cluster size dependences of bombardment effects using mass-selected gas cluster ion beams, Nucl. Instruments Methods Phys. Res. Sect. B Beam Interact. with Mater. Atoms. 261 (1-2) (2007) 660–663, https://doi.org/10.1016/j.nimb.2007.04.268.
[35] M.P. Seah, Universal equation for argon gas cluster sputtering yields, J. Phys. Chem. C. 117 (24) (2013) 12622–12632, https://doi.org/10.1021/jp402684c.
[36] L. Pan, B.K. Rao, A.K. Gupta, G.P. Das, P. Ayyub, H-substituted anionic carbon clusters CnH− (n⩽10): Density functional studies and experimental observations, J. Chem. Phys. 119 (2003) 7705–7713, https://doi.org/10.1063/1.1609400.
[37] A. Delcorte, V. Delmez, C. Dupont-Gillain, C. Lauzin, H. Jefford, M. Chundak, C. Poleunis, K. Moshkunov, Large cluster ions: soft local probes and tools for organic and bio surfaces, Phys. Chem. Chem. Phys. 22 (31) (2020) 17427–17447, https://doi.org/10.1039/D0CP02398A.
[38] C. Noël, Y. Busby, N. Mine, L. Houssiau, ToF-SIMS Depth Profiling of Organic Delta Layers with Low-Energy Cesium Ions: Depth Resolution Assessment, J. Am. Soc. Mass Spectrom. 30 (8) (2019) 1537–1544, https://doi.org/10.1007/s13361-019-02224-4.
[39] B. Saha, P. Chakraborty, MCsn+-SIMS: An Innovative Approach for Direct Compositional Analysis of Materials without Standards, Energy Procedia. 41 (2013) 80–109, https://doi.org/10.1016/j.egypro.2013.09.009.
[40] W. Xie, I. Haider Abidi, Z. Luo, L.-T. Weng, C.-M. Chan, Characterization of the interaction between graphene and copper substrate by time-of-flight secondary ion mass spectrometry, Appl. Surf. Sci. 544 (2021), 148950, https://doi.org/10.1016/j.apsusc.2021.148950.
[41] H. Chou, A. Ismach, R. Ghosh, R.S. Ruoff, A. Dolocan, Revealing the planar chemistry of two-dimensional heterostructures at the atomic level, Nat. Commun. 6 (2015) 7482, https://doi.org/10.1038/ncomms8482.
[42] N. Wehbe, J.-J. Pireaux, L. Houssiau, XPS Evidence for Negative Ion Formation in SIMS Depth Profiling of Organic Material with Cesium, J. Phys. Chem. C. 118 (46) (2014) 26613–26620, https://doi.org/10.1021/jp501851f.